

INTERNATIONAL WORKSHOP ON FAST CHERENKOV DETECTORS
PHOTON DETECTION, DIRC DESIGN AND DAQ
SEPTEMBER 11–13, 2019, GIESSEN, GERMANY

Fast readout and performance of the upgraded HADES RICH in heavy ion collisions

J. Förtsch,^{a,1} J. Adamczewski-Musch,^d M. Becker,^b M. Faul,^d J. Friese,^e C. Höhne,^{b,d}
K.-H. Kampert,^a I. Kres,^a S. Lebedev,^b S. Linev,^d J. Michel,^c J.-H. Otto,^b V. Patel,^a C. Pauly,^a
D. Pfeifer,^a E. Schwab,^d M. Traxler,^d A. Weber^b and P. Zumbach^d for the
HADES Collaboration

^aBergische Universität Wuppertal,
Gaußstraße 20, 42119 Wuppertal, Germany

^bJustus-Liebig Universität,
Heinrich-Buff-Ring 16, 35392 Gießen, Germany

^cGoethe Universität Frankfurt,
Max-von-Laue-Str. 1, 60438 Frankfurt am Main, Germany

^dGSI Helmholtz Center for Heavy Ion Research,
Planckstraße 1, 64291 Darmstadt, Germany

^eTechnische Universität München,
James-Frank-Str. 1, 85748 Garching, Germany

E-mail: j.foertsch@uni-wuppertal.de

ABSTRACT: The HADES Experiment (High Acceptance DiLepton Spectrometer) aims to measure baryonic matter at high densities but moderate fireball temperatures using heavy ion collisions. In a recent Ag+Ag beamtime, at an incident energy of 1.58 A GeV, 15.268×10^9 events have been collected at triggered event rates of 16–18 kHz. The data were recorded with the upgraded RICH detector, including the newly developed DiRICH readout chain and using HAMAMATSU H12700 MAPMTs as photon detector. In this article, we demonstrate the success of this upgrade and present first result on timing precision of the full HADES RICH detector.

KEYWORDS: Cherenkov detectors; Performance of High Energy Physics Detectors; Front-end electronics for detector readout; Instrumentation and methods for heavy-ion reactions and fission studies

¹Corresponding author.

Contents

1	The HADES RICH Detector	1
2	Performance of the RICH detector	2
2.1	Ring centre distribution	2
2.2	Ring radius distribution and number of hits per ring	3
2.3	Impact of the RICH detector on the β vs. momentum distribution	5
3	Timing precision of the RICH detector	5
3.1	Timing precision against event trigger	6
3.2	Timing precision between channel pairs	6
4	Conclusion	8

1 The HADES RICH Detector

The HADES experiment setup [1], at the GSI SIS18/FAIR facility in Darmstadt is comprised of the following components:

- A fixed Ag target consisting of 15 separated segments.
- A diamond in-beam detector system [2] (START detector) for interaction reference time measurement.
- A Ring-Imaging Cherenkov (RICH) detector with a gaseous radiator for electron identification.
- Two sets of Multiwire Drift Chambers (MDC) before and after a magnetic field region to retrieve particle momentum.
- A combined system of a scintillator-based time-of-flight wall (TOF) and a wall of resistive plate chambers (RPC) to measure the particle velocity $\beta = \frac{v}{c}$.

In March 2019 HADES was granted a Ag+Ag beamtime at an incident energy of 1.58 A GeV collecting 15.268×10^9 events at triggered event rates of 16–18 kHz. The upgraded HADES RICH [3] (as shown in figure 1) measures single photons from Cherenkov radiation with 428 HAMAMATSU H12700 multianode photomultiplier tubes (MAPMTs) distributed over a circular area of 2.65 m². The Cherenkov radiation emitted in the C₄H₁₀ isobutane radiator gas reaches the photon detection plane via a spherical mirror. As the focal plane of the spherical mirror is slightly curved, the photon detection plane is split into two sub-planes with different indentations. Here the inner plane towards low azimuthal angles θ is moved 10 cm along the beam axis towards the mirror.

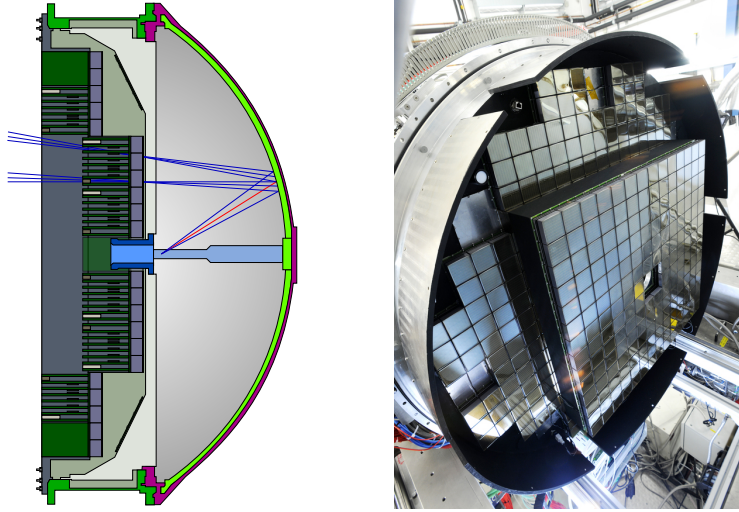


Figure 1. Left: schematic view of the HADES RICH showing a lateral cut through the centre of the detector with the beam entering from the left. The MAPMTs are placed upstream of the target with the DiRICH readout behind and the spherical mirror to the right with an electron being indicated as red line. Right: real life picture of the photon detection plane of the upgraded RICH (Photo by G. Otto GSI).

The index of refraction of isobutane guarantees that the RICH is hadron-blind due to the limited momentum range at the given collision energy.

The H12700 MAPMTs have 64 channels each for a total of 27392 channels over the full detector. Those channels are individually read out with the DiRICH readout system. This system groups the read out of always 3×2 MAPMTs where 12 DiRICH-front-end boards (DiRICH-FEBs) measure the leading edge and the time-over-threshold (ToT) of any detected pulse. One of those bundles is presented in figure 2. The DiRICH-FEBs are connected to the MAPMTs via a printed circuit board (PCB) called backplane. This backplane further works as a gas and light-tight seal between the gas filled inside of the detector and the outside. The data of those 384 channels per backplane is forwarded to the combiner module where it is then streamed to the later readout stages. Furthermore the combiner module distributes the trigger to all DiRICH-FEBs on the same backplane. The last component in this bundle is the power module, which is used for high and low voltage distribution for a full backplane module.

2 Performance of the RICH detector

In this section the performance of the RICH detector during the March 2019 beamtime will be discussed. First, the RICH intrinsic key observables such as number of hits per ring, ring radii and ring centre distributions are presented. Then, the impact of the RICH observables on the full experimental data analysis will be discussed in form of β vs. momentum distributions.

2.1 Ring centre distribution

One key aspect of any RICH detector is its homogeneous ring coverage. A good first check to find inhomogeneities in a RICH detector is to check the ring centre distribution. Here one expects a

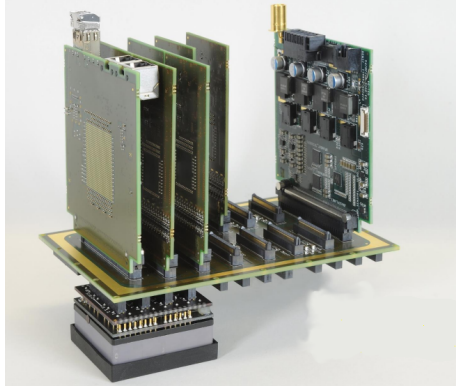


Figure 2. Photo of one DiRICH backplane bundle featuring (from left to right) the combiner module, six of twelve DiRICH-FEBs and the power module. On the other side of the backplane one out of six MAPMTs is plugged on.

smooth distribution ranging from high ring coverage in the inner part of the detector (small azimuthal angle θ) to low ring coverage in the outer part of the detector. The ring centre coverage should thus be homogeneous for each azimuthal angle θ individually. One exception to this homogeneity is to be expected for every polar angle $\phi_i = i \times 60^\circ$,¹ where the shadow of the magnetic coil cases make track reconstruction impossible. This behaviour is visible in figure 3, where the spatial ring centre distribution of the RICH is shown. The ring centres in the figure are plotted only for rings matched to an e^- or e^+ candidate track identified by the tracking and time-of-flight systems. In the figure, one can see a homogeneous ring coverage within the acceptance of other contributing detectors.

2.2 Ring radius distribution and number of hits per ring

The performance of the detector may also be checked by comparison to simulation. Two straightforward observables are the expected number of hits per ring and ring radius distribution. Comparing these two distributions to analysis results from measured data reflects the validity of simulation parameters with respect to individual MAPMT and readout parameters of the full detector. The comparison between measured and simulated ring radii is visualised in figure 4. Here one can see the comparability between simulated and measured data, as both figures show an average ring radius of 22 mm with a dependence on the azimuthal angle θ due to spherical aberrations of the mirror optics. Also visible is the sudden increase in the ring radius from inner to outer RICH photon detection plane at an azimuthal angle of $\theta \approx 48^\circ$ which reflects the two sub-planes different indentations.

The number of hits per ring is shown in figure 5. Here again simulated and measured data are in good agreement, as the average number of hits per ring differs only by one hit, having 16 hits in average per ring in measured data. The two distributions differ mainly in their width, which is slightly broader for the analysis of the measured data. The tail towards higher number of hits per ring can be attributed to misidentified double rings, which do not exist in a bare single electron simulation as presented here. Neglecting this contribution of double rings, one can assume that the

¹Where $i \in \mathbb{N}$.

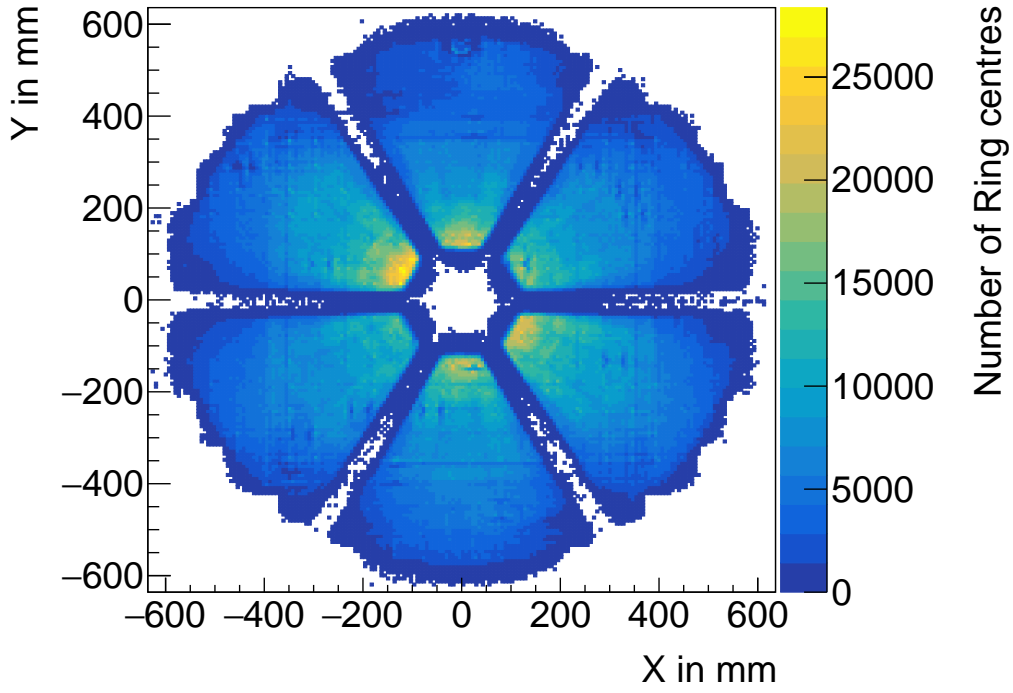


Figure 3. Spatially resolved ring centre distribution.

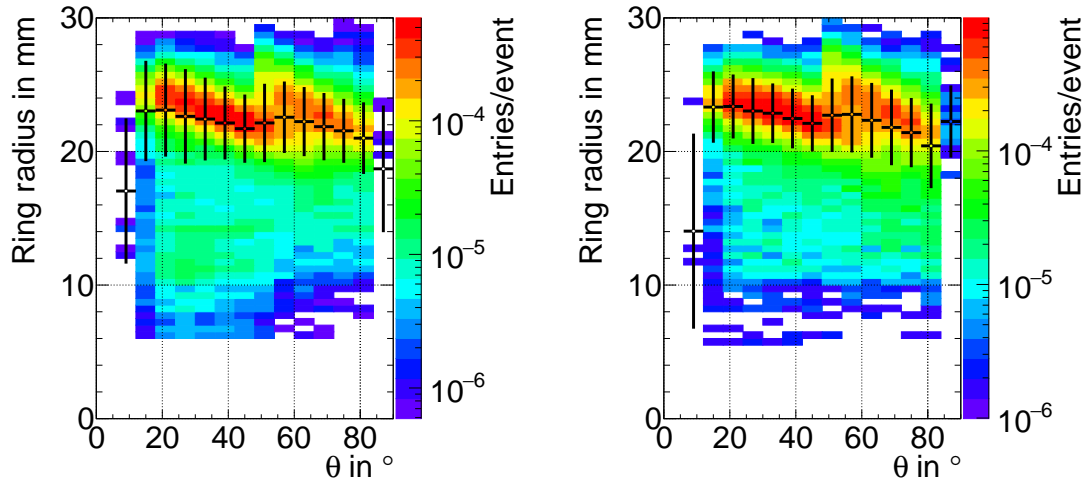


Figure 4. Ring radius distribution in terms of azimuthal angle θ for measured (left) and simulated (right) data. The points indicate the average radius per bin in θ with the error bars representing the standard error on the mean.

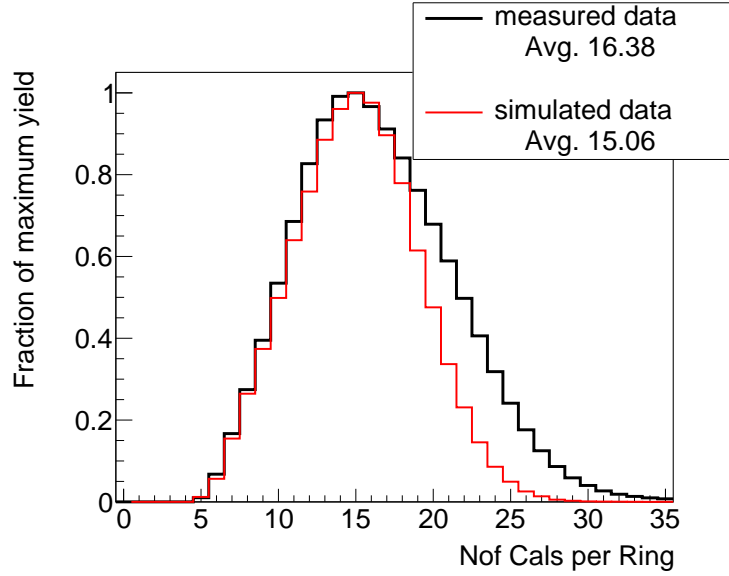


Figure 5. Distribution of number of hits per ring for measured and simulated data. Both datasets are scaled to their maximum bin content.

average number of hits per ring from measured data decreases to at least the number of hits per ring from simulated data.

2.3 Impact of the RICH detector on the β vs. momentum distribution

As the HADES RICH detector only identifies e^- or e^+ a look onto a β vs. momentum spectrum can serve as a good first probe to identify purity and efficiency. The velocity $\beta = \frac{v}{c}$ is retrieved via time-of-flight, and the momentum via track bending in the magnetic field. Requiring an identified particle in the RICH detector, the whole β vs. momentum spectrum needs to show a clear signal in the electron region around $\beta = 1$. This can be seen in figure 6 where the β vs. momentum spectrum is shown with and without requiring a RICH identified particle. The clearly visible electron region with high suppression of the previously visible π^\pm and proton branches in the spectrum demonstrates the good pion suppression capabilities of the RICH.

3 Timing precision of the RICH detector

This section focuses on the average timing precision of all channels in the RICH detector. The timing precision is derived using two different approaches: the first approach measures the time between the event trigger, as retrieved by the in-beam diamond detector in front of the targets, against the time of registered Cherenkov photon hits in all individual channels. The timing precision of each individual channel is then defined as the standard deviation of this time difference distribution. The second method uses the hit time difference between two channels that did see the same Cherenkov ring. This measure is unaffected by the event trigger timing. The standard deviation of the resulting time difference distribution for each channel pair divided by $\sqrt{2}$ is used as measure of the timing precision for each of the two channels in this pair.

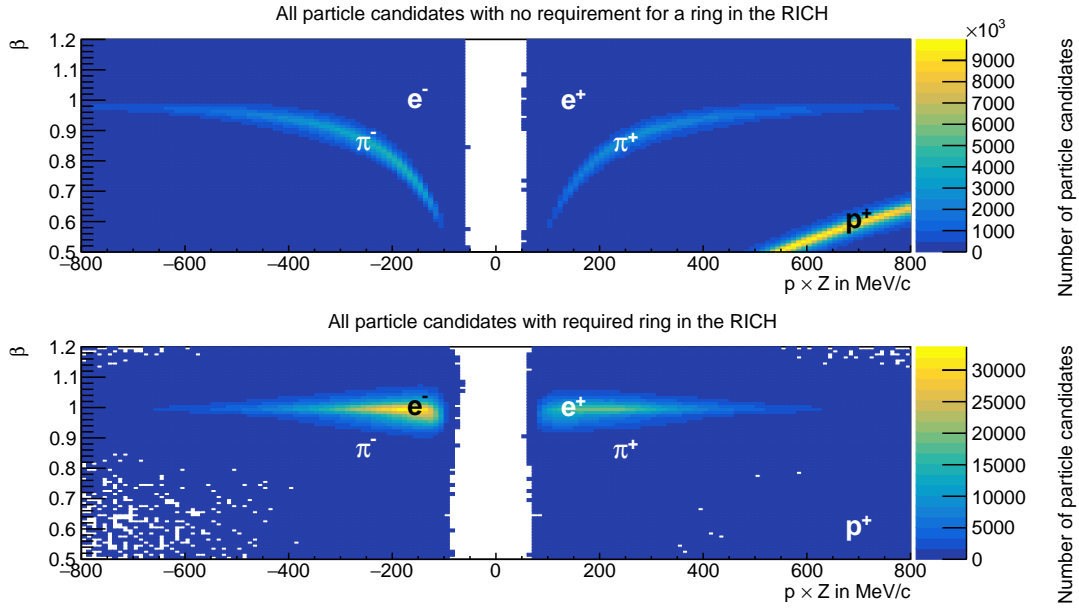


Figure 6. Velocity vs. momentum distribution with (bottom) and without (top) requiring a Cherenkov ring in the RICH detector. For correct ring identification the ring needs to have a radius between 17 mm and 30 mm using tight cuts on time-over-threshold (ToT) and photon hit time for each channel individually.

3.1 Timing precision against event trigger

To retrieve the timing precision of a single channel, all hits seen by this channel that stem from rings correlated to an e^\pm -candidate are used. Those hits additionally need to have a time-over-threshold (ToT) of ± 0.05 ns around the channel's average single photon ToT value. In this way any artificial broadening of the resulting timing distribution due to walk effects from different signal amplitudes and hence ToTs² is suppressed. The selected hits are filled into one-dimensional histograms for each channel. These histograms each feature a distinct Gaussian distribution. The standard deviation of each distribution is then used as an estimate for the timing precision of the particular channel. As not all channels see enough hits from rings correlated to an e^\pm -candidate due to lower ring densities in the outer detector regions, those predominantly outer channels are disregarded in the further timing analysis. The distribution of all single channel timing precision values is depicted in figure 7 on the left side. The average timing precision of the full detector using this approach is found to be 221 ps. The obtained result is still folded with the timing precision of the START detector which is used as the event trigger. This influence is considered to be small due to the good timing precision of the START detector, in the order of 50 ps [4]. The achievable timing precision is limited by the MAPMT properties in terms of the Transit-Time Spread (TTS) in the order of 150 ps.

3.2 Timing precision between channel pairs

The second approach uses the measured time differences between individual Cherenkov photon hits within one ring. Here, all channel pairs are taken, that detected hits from the same ring

²The amplitude dependant time-walk is not yet corrected for in the standard analysis chain, but will later be corrected based on the ToT measurement.

being correlated to an e^\pm -candidate. The time between the two hits is thus independent of the event trigger and only influenced by variances in the DiRICH time-to-digital converter chain and channel-individual offsets. Also in this analysis, the ToT influences the timing of each individual channel due to walk effects. Since both photons in each channel pair are now measured by the RICH, this influence can be partially eliminated by only comparing single photon hits which have similar ToT and thus amplitude. A cut on a maximum ToT difference of 0.5 ns is applied in order to minimise the influence of time-walk on the result. However, even with this limit on the ToT, the still persistent walk in this ToT-window will worsen the timing precision more strongly as compared to the single channel analysis. Also in this method the time difference distribution for each channel pair follows a Gaussian shape which allows for extraction of the standard deviation via fit. As before, to derive the average detector timing precision, the standard deviations of all individual channel pairs across the whole detector are combined into one histogram. This histogram is depicted in figure 7 on the right side. Channel pairs without enough coinciding hits are not taken into account. This method results in an upper limit of 226 ps for the average timing precision of the full detector. The remaining broadening in this result due to time-walk is estimated to be in the order of 20 ps.³

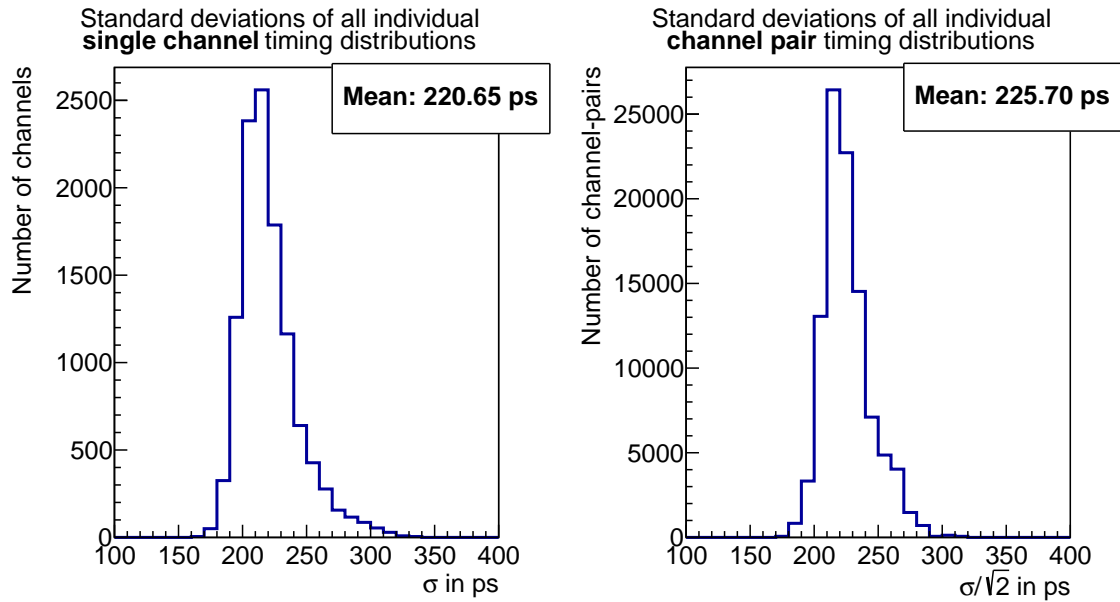


Figure 7. Left: standard deviations of the time difference distribution for each channel against the event trigger. Right: standard deviations of the channel pair time difference distribution for each channel pair seeing the same rings from e^\pm -candidates. Here the channel pair standard deviation is divided by $\sqrt{2}$ to show the channel-individual standard deviation, assuming that both channels contribute equally to the standard deviation of the channel pair. For this histogram, the number of entries reflects the number of channel pairs with a reasonable number of simultaneous hits.

³According to a linear extrapolation, loosening the cut on the maximum ToT difference.

4 Conclusion

This article shows the good performance of the upgraded HADES RICH during the March 2019 beamtime. This conclusion is drawn from a homogeneous ring centre distribution and a clear reduction of all hadronic components in the β vs. momentum distribution requiring a correctly identified Cherenkov ring in the RICH. Good agreement between measured and simulated data of low-level observables, such as number of hits per ring and spatial ring radius distribution, is presented. An average timing precision of 230 ps and below across the full detector is achieved using the presented analysis method for a small ToT bin.

Acknowledgments

The authors would like to thank the TRB working group⁴ for their support realising and setting up the readout chain for the HADES RICH.

The work described in this article was supported by the Bundesministerium für Bildung und Forschung, under grant number BMBF 05P15PXFCA, BMBF 05P19PXFCA, BMBF 05P15RGFCA and BMBF 05P19RGFCA, HGS-HIRe.

References

- [1] HADES collaboration, *The High-Acceptance Dielectron Spectrometer HADES*, *Eur. Phys. J. A* **41** (2009) 243 [[arXiv:0902.3478](#)].
- [2] J. Pietraszko, L. Fabbietti, W. Koenig and M. Weber, *Diamonds as timing detectors for MIP: The HADES proton-beam monitor and start detectors*, *Nucl. Instrum. Meth. A* **618** (2010) 121 [[arXiv:0911.0337](#)].
- [3] C. Pauly et al., *Upgrade of the HADES RICH photon detector with H12700 MAPMTs*, *Nucl. Instrum. Meth. A* **876** (2017) 164.
- [4] A. Rost et al., *Performance of the CVD Diamond Based Beam Quality Monitoring System in the HADES Experiment at GSI**, in *Proceedings of IPAC*, Melbourne, Australia, 19–24 May 2019, pp. 2507–2509.

⁴trb.gsi.de